INTERNATIONAL JOURNAL OF
RADIATION ONCOLOGY • BIOLOGY • PHYSICS
www.redjournal.org

BIOLOGY OR PHYSICS CONTRIBUTION

Neutron Capture Enhances Dose and Reduces Cancer Cell Viability in and out of Beam During Helium and Carbon Ion Therapy

Nicholas Howell, BSc,[*] Ryan J. Middleton, PhD,[*] Frederic Sierro, PhD,[*] Benjamin H. Fraser, PhD,[*] Naomi A. Wyatt, BSc,[*] Andrew Chacon, PhD,[*] Keith R. Bambery, PhD,[*] Elle Livio, PhD,[*] Christopher Dobie, PhD,[*] Joseph J. Bevitt, PhD,[*] Justin Davies, PhD,[*] Anthony Dosseto, PhD,[†] Daniel R. Franklin, PhD,[‡] Ulf Garbe, PhD,[*] Susanna Guatelli, PhD,[§] Ryoichi Hirayama, PhD,[‖] Naruhiro Matsufuji, PhD,[‖] Akram Mohammadi, PhD,[‖] Karl Mutimer, BA,[*] Louis M. Rendina, PhD,[¶,#] Anatoly B. Rosenfeld, PhD,[§] and Mitra Safavi-Naeini, PhD[*,§]

[*]*Australian Nuclear Science and Technology Organisation, Lucas Heights, Australia;* [†]*Wollongong Isotope Geochronology Laboratory, School of Earth, Atmospheric and Life Sciences, University of Wollongong, Wollongong, Australia;* [‡]*School of Electrical and Data Engineering, University of Technology Sydney, Ultimo, Australia;* [§]*Centre for Medical Radiation Physics, University of Wollongong, Wollongong, Australia;* [‖]*National Institutes for Quantum Sciences and Technology, Chiba, Japan;* [¶]*School of Chemistry, The University of Sydney, Sydney, Australia; and* [#]*The University of Sydney Nano Institute, Sydney, Australia*

Received May 7, 2023; Accepted for publication Feb 24, 2024

Purpose: Neutron capture enhanced particle therapy (NCEPT) is a proposed augmentation of charged particle therapy that exploits thermal neutrons generated internally, within the treatment volume via nuclear fragmentation, to deliver a biochemically targeted radiation dose to cancer cells. This work is the first experimental demonstration of NCEPT, performed using both carbon and helium ion beams with 2 different targeted neutron capture agents (NCAs).

Methods and Materials: Human glioblastoma cells (T98G) were irradiated by carbon and helium ion beams in the presence of NCAs [^{10}B]-BPA and [^{157}Gd]-DOTA-TPP. Cells were positioned within a polymethyl methacrylate phantom either laterally

Corresponding author: Mitra Safavi-Naeini, PhD; E-mail: mitras@ansto.gov.au

Disclosures: none. This work was partly funded by the Yamagiwa-Yoshida Memorial International Cancer (YY) grant, which provided the necessary funding for traveling and carrying out experiments at the National Institute for Quantum Science and Technology's Heavy Ion Medical Accelerator Chiba (HIMAC, QST). A.C. was beneficiary of an Australian Government Research Training Program Scholarship. This work was supported by the Australian Nuclear Science and Technology Organisation (ANSTO) and the Japanese National Institutes for Quantum Science and Technology (QST). The project received additional support from the Japan National Committee for the Union for International Cancer Control (UICC-Japan), the University of Sydney's Drug Discovery Initiative (DDI), and the Australian Institute for Nuclear Science and Engineering (AINSE). Access to the Australian Centre for Neutron Scattering (ACNS) was enabled by the National Collaborative Research Infrastructure Strategy of Australia (NCRIS) in supporting the neutron research infrastructure used in this work via ACNS proposals P7928 and DB6388.

Data Sharing Statement: All data generated or analyzed during this study and all simulation and analysis code included in the paper and its Supplementary Information files are available for download from the following public repository: https://bitbucket.org/mitra_safavi/ncept-invitro-data/. These include a complete database of the raw neutron fluence measurements and gold activity (per foil), and the resazurin fluorescence measurements colony count, Monte Carlo simulation code and data analysis code, and the cell colony counting scripts used in the classification and identification of the cell colonies.

Acknowledgments—We would like to thank Gabriele Enge from the Wollongong Isotope Geochronology Laboratory (WIGL) for advice and technical support on ICP-MS analysis. We thank Hitomi Sudo and Atsushi Tsuji from the Institute for Quantum Medical Sciences (iQMS) for facilitating access to crucial analytical equipment for experiments conducted at QST. We acknowledge NST Biosciences (ANSTO) for providing laboratory space and consumables for the development of the in vitro cell based models. Computer simulations were supported by the National Computing Merit Allocation Scheme (NCMAS) and the Multimodal Australian Sciences Imaging and Visualisation Environment (MASSIVE). Invaluable support and advice were provided by the beam operators and technicians at the Heavy Ion Medical Accelerator (HIMAC) in Chiba, Japan, and all experiments were enabled via merit access as an approved research project with heavy ions at QST-HIMAC.

Supplementary material associated with this article can be found, in the online version, at doi:10.1016/j.ijrobp.2024.02.052.

https://doi.org/10.1016/j.ijrobp.2024.02.052

adjacent to or within a 100 × 100 × 60 mm spread out Bragg peak (SOBP). The effect of NCAs and location relative to the SOBP on the cells was measured by cell growth and survival assays in 6 independent experiments. Neutron fluence within the phantom was characterized by quantifying the neutron activation of gold foil.

Results: Cells placed inside the treatment volume reached 10% survival by 2 Gy of carbon or 2 to 3 Gy of helium in the presence of NCAs compared with 5 Gy of carbon and 7 Gy of helium with no NCA. Cells placed adjacent to the treatment volume showed a dose-dependent decrease in cell growth when treated with NCAs, reaching 10% survival by 6 Gy of carbon or helium (to the treatment volume), compared with no detectable effect on cells without NCA. The mean thermal neutron fluence at the center of the SOBP was approximately 2.2×10^9 n/cm^2/Gy (relative biological effectiveness) for the carbon beam and 5.8×10^9 n/cm^2/Gy (relative biological effectiveness) for the helium beam and gradually decreased in all directions.

Conclusions: The addition of NCAs to cancer cells during carbon and helium beam irradiation has a measurable effect on cell survival and growth in vitro. Through the capture of internally generated neutrons, NCEPT introduces the concept of a biochemically targeted radiation dose to charged particle therapy. NCEPT enables the established pharmaceuticals and concepts of neutron capture therapy to be applied to a wider range of deeply situated and diffuse tumors, by targeting this dose to microinfiltrates and cells outside of defined treatment regions. These results also demonstrate the potential for NCEPT to provide an increased dose to tumor tissue within the treatment volume, with a reduction in radiation doses to off-target tissue.

Introduction

Radiation therapy aims to treat cancer by delivering a therapeutic dose to the entire tumor while minimizing radiation exposure to healthy tissue. Of the various radiation therapy methods, charged particle therapy (either proton or heavy ion therapy[1-4]) is among the most effective at achieving this goal. This is because charged particles can deliver a highly conformal radiation dose with a small number of treatment fractions, even to deep tumors, because of the physical characteristics of an ion's Bragg peak. The energy loss of a charged particle is inversely proportional to the square of its velocity, resulting in the majority of its kinetic energy being deposited at the end of its track just before it comes to rest.

The effectiveness of charged particle therapy is limited by the accuracy with which the tumor can be delineated during preirradiation positron emission tomography/computed tomography or positron emission tomography/magnetic resonance imaging, because unresolvable microinfiltrates and micrometastasis cannot be deliberately targeted for irradiation. Furthermore, although the entrance dose — the dose received by tissue through which the beam passes before reaching the tumor — is lower than for photon therapy, it remains substantial and must be carefully limited during treatment planning. Additionally, inelastic collisions between accelerated charged particles and the target result in a range of nuclear fragments, including lighter ions and neutrons that deposit additional dose in surrounding tissues.[2] The neutron component of this radiation field extends almost isotropically around the target volume, and because of scattering within the patient, the neutrons rapidly lose kinetic energy and approach thermal equilibrium with their surroundings.[4,5]

An extension of charged particle therapy that utilizes the neutron component of the radiation field within the patient via neutron capture was proposed in 2018 (Fig. 1). Neutron capture therapy (NCT) has been previously used for cancer treatment by systemic administration of a neutron capture agent (NCA) to the patient and irradiating the target tissue with an external neutron source. In NCT, thermal neutrons are captured by isotopes with high thermal neutron capture cross-sections, releasing high-linear energy transfer (LET) charged particles that damage cancer cells.[6-9] However, the use of an external neutron source limits the depth at which sufficient neutrons can be delivered to the target without causing excessive radiation-induced proximal tissue injury.

Neutron capture enhanced particle therapy (NCEPT) aims to combine the spatial precision of charged particle therapy with the precise biochemical targeting of NCT. NCEPT offers 2 major benefits compared with conventional charged particle therapy:

1. The dose to the target volume can be increased relative to the surrounding tissue (including the entrance region) because of the additional contribution of the neutron capture dose.
2. Because the neutron field is generated internally and extends beyond the primary treatment volume, a biochemically targeted NCA that preferentially concentrates in cancer cells can deliver a therapeutically useful dose even to small satellite lesions beyond the primary target volume.

The theoretical feasibility of this method has previously been established via Monte Carlo simulations, demonstrating that a representative proton or heavy ion therapy treatment plan will generate a sufficient thermal neutron field to deliver an additional dose of at least 10% with achievable tissue concentrations of both ^{10}B- and ^{157}Gd-based NCAs.[10] Although dose enhancement has previously been reported experimentally during proton therapy in the presence of natural boron by Cirrone et al[11] and Bláha et al[12] and attributed to proton-^{11}B fusion, it now appears that the vast majority of this effect is actually due to neutron capture by

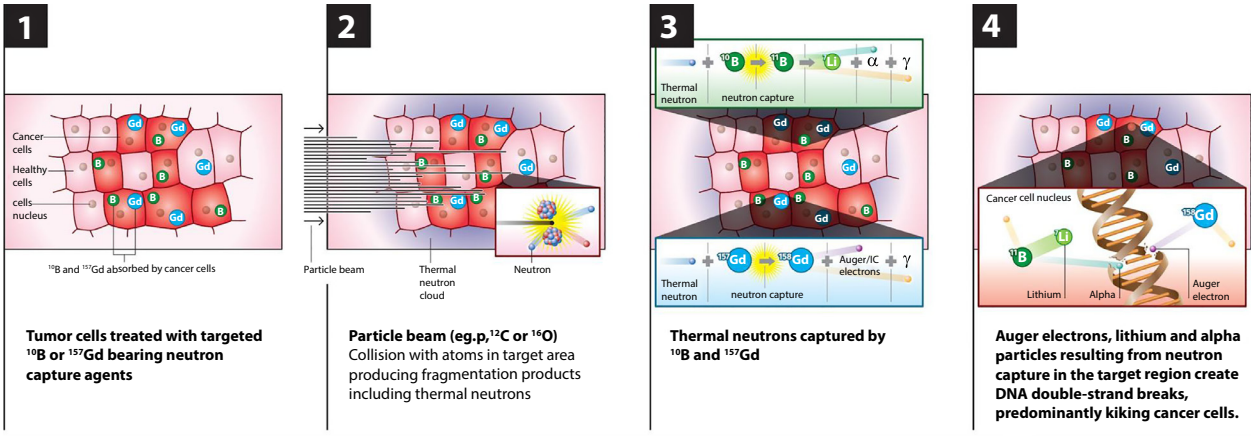

Fig. 1. Physics of neutron capture enhanced particle therapy. As ions in the beam traverse tissues proximal to the target, some undergo nuclear interactions with target matter, creating a variety of nuclear fragmentation products, including neutrons, which disperse in the body and thermalize. Target-specific agents deliver ^{10}B or ^{157}Gd payloads to cancer cells, where thermal neutrons are captured, resulting in emission of short-range (4-8 μm for ^{10}B, 10-20 nm for ^{157}Gd), high-linear energy transfer particles. Although the particle beam treats the bulk of the tumor, the neutrons released are captured anywhere that neutron capture agents are present - inside and outside the primary treatment volume - that would have otherwise remained unirradiated.

^{10}B,[13,14] which has a natural isotopic abundance of 19.8%,[15] rather than proton-^{11}B fusion (with Jacobsen et al[13] reporting that the number of high-LET particles produced by neutron capture outnumber those produced via fusion by a ratio of ~4000 ± 700:1). This hypothesis is especially supported strongly by the failure of the result to be reproduced experimentally in the absence of a surrounding phantom (which is necessary to generate a neutron field but should not be necessary for proton-^{11}B fusion).[16,17] Therefore, if neutron capture is the dominant cause of dose enhancement, then the effect should also be observed during helium or carbon ion therapy in the presence of enriched ^{10}B (or other high neutron capture cross-section isotopes such as ^{157}Gd), where proton fusion plays no role whatsoever.

In this paper, the NCEPT principle is established in vitro using 2 NCAs irradiated by helium and carbon ions. The first, 4-borono-L-phenylalanine ([^{10}B]BPA; Fig. 2a) is an unnatural amino acid that has been used clinically in conventional neutron capture therapy for more than 2 decades.[18] BPA is transported primarily through amino acid transporter LAT1, and, to a lesser extent, LAT2 and ATB(0+).[19] LAT1 is a plasma membrane amino acid transporter that is expressed in a variety of cancer tissues, and high expression is associated with poor prognosis.[20] ^{10}B has a high capture cross-section for thermal neutrons (~3800 barns). Upon capturing a thermal neutron, an excited ^{11}B* nucleus is formed, which immediately decays to release 2 high LET ions — an α particle and a + ^{7}Li nucleus[21] — with ranges of approximately 4.1 and 7.7 μm in tissue, respectively.

The second NCA is the novel compound 2,2′,2″-[10-{2-[(triphenylphosphonio)methyl]benzyl}- 1,4,7,10-

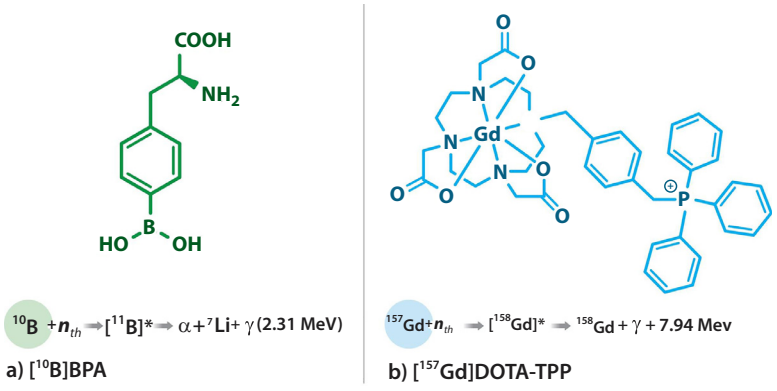

Fig. 2. Neutron capture agents used in this work and their respective thermal neutron capture reactions. (a) ^{10}B-enriched 4-borono-L-phenylalanine; (b) ^{157}Gd-enriched 2,2′,2″-[10-{2-[(triphenylphosphonio)methyl]benzyl}-1,4,7,10-tetraazacyclododecane-1,4,7-triyl]triacetatogadolinium(III) trifluoroacetate.[34,42]

tetraazacyclododecane-1,4,7-triyl]triacetatogadolinium(III) trifluoroacetate ([^{157}Gd]DOTA-TPP; Fig. 2b), which uses the mitochondria-targeting moiety triphenylphosphonium (TPP) to accumulate ^{157}Gd in the inner mitochondrial membrane. TPP is particularly efficient at accumulating in negatively charged membrane compartments.[22] This compound preferentially accumulates in cancer cells because of the increased mitochondrial function in many cancers.[23-25] ^{157}Gd is a stable isotope of gadolinium with an extremely high thermal neutron capture cross-section ($\sim 2.55 \times 10^5$ barns). Neutron capture by ^{157}Gd results in the formation of an excited ^{158}Gd* nucleus; its subsequent de-excitation results in the emission of an average of 5 Auger and 0.69 internal conversion electrons, plus an average of 1.8 high energy prompt γ photons and 1 recoil ^{158}Gd nucleus.[26-29] The high LET Auger electrons have a range of the order of 10 to 20 nm; accumulation of damage to the inner mitochondrial membrane will, in most cases, lead to apoptosis.[30]

Demonstrated in the following sections is the effect of NCEPT on human glioblastoma multiforme cell culture when irradiated with helium and carbon ion beams, emphasizing the potential significance of including neutron capture to the treatment volume itself as well as the surrounding area in the overall treatment plan.

Methods and Materials

The experiments described in the following sections have 3 primary objectives:

1. Confirming the magnitude and distribution of the predicted thermal neutron fluence in and around the primary radiation field (target volume)
2. Determining whether the results predicted via the previous simulation study would translate to effective attenuation of cancer cell proliferation in vitro, using ^{4}He and ^{12}C ion beams and 2 neutron capture agents
3. Determining the effect of neutron capture on cancer cells outside of the primary radiation field but still within the thermal neutron field generated by the heavy ion irradiation

The experimental configuration is shown in Figure 3. All experimental measurements were performed using the Heavy Ion Medical Accelerator in Chiba biologic beamline at the National Institute for Quantum Science and Technology in Japan.

Phantom and irradiation conditions

A multilayer cubic polymethyl methacrylate (PMMA) phantom (ρ = 1.19 g/cm^3) was assembled with total dimensions of 300 × 300 × 300 mm^3. PMMA slab inserts were constructed with either paired circular indentations for holding gold foils or with single or double cut outs for holding T25 flasks filled with medium (Fig. 3). The cut outs for the T25 flasks were positioned so that the cell layer (at the bottom of the flasks) was located at depth Z_2 (100 mm) in PMMA, perpendicular to the beam.

For both carbon and helium ion beams, a 100 × 100 × 60 mm^3 spread-out Bragg peak (SOBP) was used, corresponding to a depth range of 80 to 140 mm in PMMA. The SOBPs were generated via passive scattering of monoenergetic 150 and 290 MeV/u helium and carbon ion beams, respectively, with the distal edges (ie, the maximum depths) of the SOBPs corresponding to the energies of the respective monoenergetic ion beams.

Thermal neutron fluence measurements

The differential neutron activation method for thermal neutron fluence measurement was validated beforehand via Monte Carlo simulations (as described in the Supplementary Materials Section 1; physics models are detailed in Table E1 and the results obtained via simulation are compared with ground truth in Tables E3 and E4).

The neutron detector consisted of pairs of thin disc foils of pure ^{197}Au (average mass = 12.075 mg; ρ = 19.32 g.cm^{-3}; nominal r = 3 mm; nominal T = 0.02218 mm); 1 disc was bare and the other was covered by a 1-mm layer of cadmium on both sides to absorb thermal neutrons. Paired foils were placed at different positions in a 5-mm thick PMMA layer, which was then inserted into the phantom at depths of 48 mm (proximal to the SOBP), 100 and 133 mm (both inside the SOBP), and 153 mm (distal to the SOBP). At each depth, foil pairs were placed at lateral offsets of -12 mm (rather than zero, so as to avoid overlap with successive depths), +50 and +100 mm from the central axis of the phantom. Additional foil pairs were placed on a radius at a 45° offset in the transaxial plane, with the pairs centered at points 70.7 and 154 mm from the center of the phantom. Therefore, each plate included a total of 5 pairs of foils. A schematic diagram of the plate outline is shown in Figure 3 (specific locations are described in Table E2). Successive plates were stacked and progressively rotated by 90° to avoid attenuation of the primary particle beam by preceding foils.

Total doses of 70 Gy(relative biological effectiveness [RBE]) and 35 Gy(RBE) were used for irradiation with helium and carbon, respectively. The resulting gold foil activities were measured over a period of 1 h using a high purity germanium detector (Canberra GC-2020), and the number of photons detected within the 411 keV γ peak were converted to thermal neutron fluence using (1):

$$\Phi_\theta = \frac{2A}{\sqrt{\pi} N_A \alpha \sigma_0 G_{th} m} \cdot \frac{T e^{\lambda\tau}}{1 - e^{-\lambda T}} \sqrt{\frac{T_n}{T_0}} \left(A_{Au}(\tau) - A_{Cd-Au}(\tau) \right) \quad (1)$$

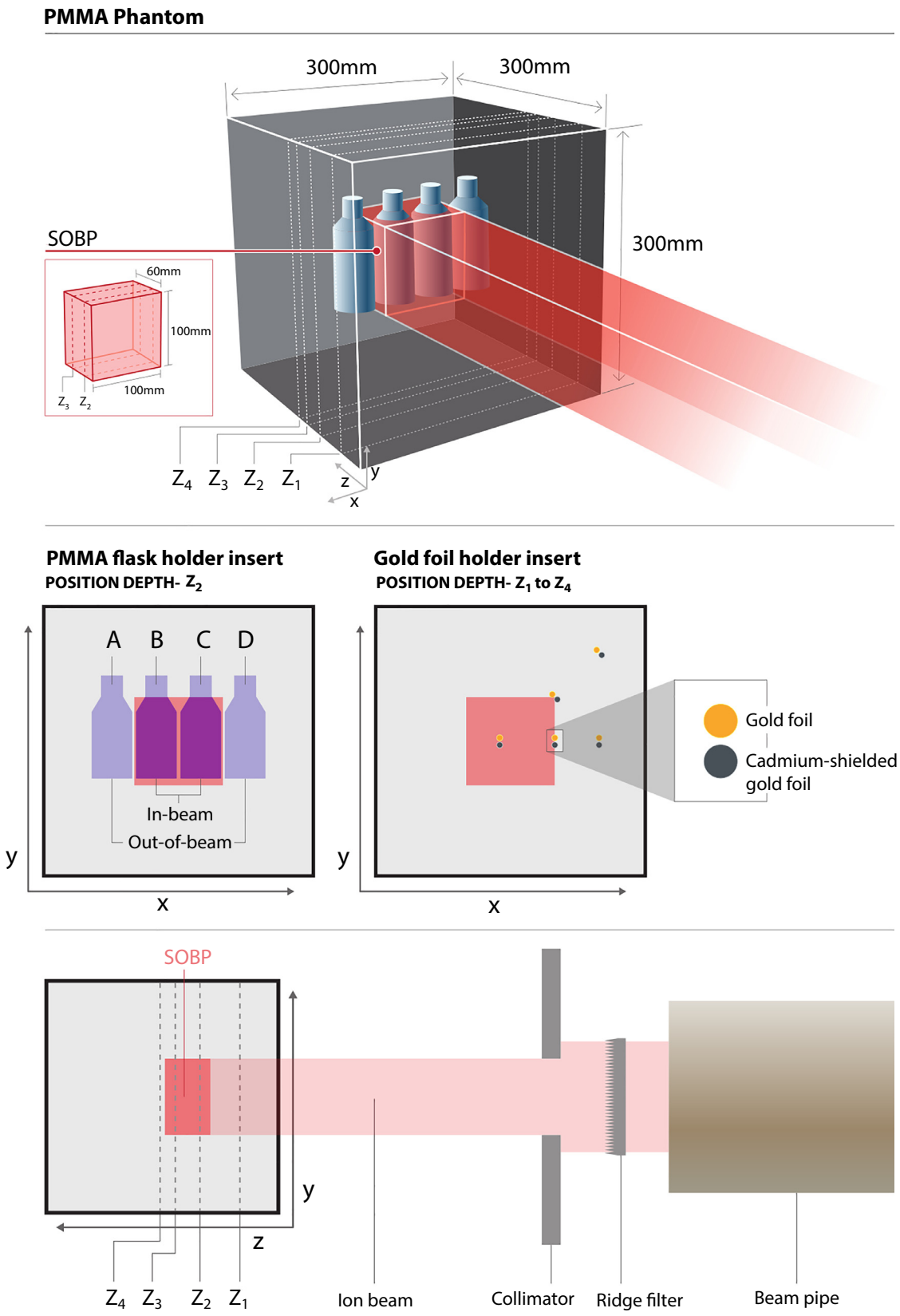

Fig. 3. Experimental configuration. Irradiation positions for flask irradiation and neutron fluence measurements. Positions (A) and (D) are out of beam; (B) and (C) are in-beam. The SOBP extends 60 mm from a depth of 80 to 140 mm (in the z dimension), with a 100 × 100-mm cross-sectional area. Gold activation measurements of thermal neutron fluence were made at depths of Z_1 = 48 mm (proximal to the SOBP), Z_2 = 100 mm (inside the SOBP), Z_3 = 133 mm (inside the SOBP), and Z_4 = 153 mm (distal to the SOBP). For further detail see Figure E1.
Abbreviation: SOBP = spread-out Bragg peak.

where τ is the time after irradiation that the measurements are performed (zero if the activity is decay-corrected), $A_{Au}(\tau)$ is the postirradiation activity of the bare gold foil (due to all neutron captures) at $t = \tau$, $A_{Cd\text{-}Au}(\tau)$ is the activity of the cadmium-shielded foil at $t = \tau$, A is the mass number of gold (assumed to be 196.9666), N_A is Avogadro's number, α is the abundance of the target isotope ^{197}Au (assumed to be 1), σ_0 is the thermal neutron cross-section of ^{197}Au (9.87×10^{-23} cm^2), G_{th} is the self-shielding ratio, m is the mass of the sample, λ is the decay constant of ^{198}Au, T is the duration of irradiation, T_n is the sample temperature, and T_0 is the reference temperature (both are 293 K in this case).[31,32] The resulting fluence estimate is divided by the biologic dose to provide the flux per unit dose (n/cm^2/Gy [RBE]).[32,33] A full derivation of the self-shielding ratio for the experimental configuration is provided in the Supplementary Materials Section 2.

Cell cultures

The human glioblastoma multiforme cell line, T98G, was sourced from the Japan Cancer Research Resources Bank. T98G was maintained as a subconfluent culture in a humidified incubator at 37 °C with 5% CO_2 grown in Eagles Modified Essential Media (EMEM; Gibco) supplemented with 10% fetal bovine serum plus penicillin and streptomycin antibiotics.

NCAs

Two neutron capture agents were used in this study: [^{10}B]BPA and [^{157}Gd]DOTA-TPP. The chemical structure of these compounds and the relevant neutron capture reactions are shown in Figure 2. [^{10}B]BPA (>98.4% ^{10}B) was purchased from Interpharma Praha. [^{157}Gd]DOTA-TPP (>88% ^{157}Gd) was synthesized using a 2-step procedure adapted from Morrison et al.[34] In brief, commercially available DO3A-*tert*-butyl ester (Macrocyclics) was alkylated with 4-(bromomethyl)benzyl)triphenyl phosphonium bromide under basic conditions to yield a solid, which was then reacted, without further purification, with trifluoroacetic acid, which cleaved the *tert*-butyl ester protecting groups. The excess trifluoroacetic acid was then removed by evaporation under reduced pressure, and the resulting crude material was purified by reverse-phase preparative high-performance liquid chromatography to give the DOTA-TPP ligand as white solid. The purified DOTA-TPP ligand was then dissolved up in water and treated with Gd-157 enriched (88%) gadolinium oxide. The final product was obtained, after filtration and lyophilization, as white solid and gave high-performance liquid chromatography (QC), elemental analysis, and mass spectrometry data consistent with that expected for the gadolinium-157 enriched metal complex ([^{157}Gd]DOTA-TPP; see Supplementary Materials Section 3 for full details).

Cell irradiation conditions

Irradiations of T98G cultures were conducted in 80% to 90% confluent T25 tissue culture flasks. Approximately 24 h before irradiation, the cultures were treated with either 500 μM [^{10}B]BPA, 500 μM [^{157}Gd]DOTA-TPP, or a vehicle control.

Carbon and helium ion beams were configured to deliver nominal dose rates of ~1 Gy/min, with exact exposure times adjusted based on nightly dose rate measurements at the beginning of each experimental session. Total doses of 0, 2, 3, 4, 6, and 8 Gy were used for irradiation of the NCA-treated and control flasks (control flasks received an additional dose of 10 Gy) for both ions. Immediately before irradiation, the flasks were topped up to the base of the neck with either phosphate-buffered saline (PBS) or EMEM. Flasks were irradiated at positions B and C, with the cell layer at a depth of 100 mm within the PMMA phantom (Fig. 3), at room temperature, either in pairs or alongside a sham flask containing only water. After irradiation (5-10 min from beam-off), the media was vacuum aspirated and the T98G monolayer detached and processed as described in the following sections for both cell growth (resazurin) and/or clonogenic assays.

To evaluate the efficacy of neutron capture events occurring outside of the primary beam field, flasks were prepared as previously discussed, with either 500 μM [^{10}B]BPA, [^{157}Gd]DOTA-TPP, or diluent control. The flasks were placed at positions A and D within the phantom, and B and C received a sham water flask. Total doses of 0, 1, 3, 6, and 10 Gy of carbon and helium ions were delivered by the primary beam to the 2 sham flasks.

The efficacy of [^{10}B]BPA and [^{157}Gd]DOTA-TPP as a function of concentration was investigated by fixing the physical dose at 3 Gy and irradiating T98G cultures under progressively decreasing concentrations of NCA. Three Gy was chosen as it is approximately equal to the LD30 for T98G cells in response to direct irradiation with the carbon or helium particle beam. A dilution series was created for each compound in EMEM (500, 250, 100, 50, 25, 10, 5, 2.5, and 1 μM) plus a vehicle control. Cells were incubated with NCA for approximately 24 h and irradiated, as described previously, with 3 Gy of carbon ions or helium ions at a dose rate of ~1 Gy/min and immediately processed as described in the following sections. A 0 Gy (minimum response) and 10 Gy (maximum response) control were also included for each NCA treatment group and vehicle control.

Cell growth assay

The resazurin reduction-based cell proliferation assay was the preferred method chosen for measuring the effect of NCEPT in vitro. It has several advantages over clonogenic assay under these conditions (especially extremely limited beamtime), including increased throughput, straightforward

data interpretation, and observability of growth kinetics including lag and plateau phases. The use of a metabolic reduction as the readout means that the assay takes into account all viable cells within a population, including those that have left the cell cycle because of radiation effect (eg, senescence, quiescence). This distinguishes this approach from the traditional clonogenic assay and leads to the production of a more conservative, but overall representative, view of the cellular effect in a nonuniform mixed radiation field. This method was employed for quantifying in-beam and out-of-beam dose response as well as the (in-beam) NCA concentration response with a fixed ion dose.

After irradiation, the cell monolayer was detached with trypsin and the resulting cell suspensions were adjusted to 2500 cells/mL; 200 μL of this suspension was pipetted into the designated wells of 7 × 96 well, black wall, clear bottom plates to give 500 cells/well. Plates were incubated at 37 °C with 5% CO_2. One plate was assayed every 24 h for viable cell mass using resazurin assay as follows.[35] A 1% w/v stock solution of resazurin sodium salt was prepared in water. The stock was diluted 250 times in PBS and warmed to 37 °C in a water bath. All media was removed from the plate, replaced with resazurin-PBS, and incubated for 60 min at 37 °C. The resulting conversion of resazurin to resorufin was measured by recording the fluorescence at excitation wavelength 555 nm and emission wavelength 585 nm at 37 °C. The resulting relative fluorescence units were plotted against time (days) to quantify the proliferation rates and growth of T98G cultures after irradiation with and without NCA[36] (Figs. E2 and 3). A timepoint was selected from these data in which all treatments were in as close to an exponential growth phase as possible (ie, 144 h) and the relative fluorescence units replotted against log dose (Gy), with 95% CIs, for each well of cells treated with either no NCA, [^{10}B]BPA, or [^{157}Gd]DOTA-TPP and irradiated with both carbon and helium ion beams. Lethal dose, 50% (LD_{50}) was determined by fitting a sigmoidal log-inhibitor versus response model to these data, and percent response (F) was calculated from this LD_{50} and the Hill-slope (H) using the relationship:

$$LD_F = \left(\frac{F}{100 - F}\right)^{\frac{1}{H}} \cdot LD_{50}$$

Clonogenic assay

Clonogenic assay was also employed as a secondary method for evaluation of in-beam cell survival in response to ion irradiation with and without the presence of NCAs.

After irradiation, flasks were trypsinized and T98G cells were seeded into Petri dishes (Falcon 100-mm Cell Culture Dish; Corning) with concentrations listed in Table E7. The cells were then incubated at 37°C with 5% CO_2 for 12 days (approximately 10 doubling times[37]). The resulting cell cultures were washed with 5 mL of PBS, fixed in 5 mL of 10% neutral buffered formalin, washed with distilled water, and stained with crystal violet to highlight the nucleus and aid with colony identification. Each dish was then left to dry and digitized using the ImageQuant LAS 4000 (GE) imaging system.[38] The number of colonies (>50 cells) in each dish was estimated using the OpenCFU software[39] (see Fig. E4). Survival fraction was then calculated by dividing the number of colonies by the initial seeding density.

The mean survival fraction was plotted on a logarithmic scale against dose, with 95% CIs, for each population of cells treated with either no NCA, [^{10}B]BPA, or [^{157}Gd]DOTA-TPP and irradiated with both carbon and helium ion beams.

The survival fraction of cells irradiated by photons or charged particles generally follows a linear-quadratic function of dose, according to the relation

$$SF = e^{-\alpha D - \beta D^2}$$

The α and β parameters were computed using a least-squares error minimization algorithm for each case (Table E8), and the 1% and 10% survival fractions were estimated for each case.

Results

Thermal neutron fluence measurements

The thermal neutron fluences at each point of measurement resulting from irradiation of the PMMA target with helium ions are plotted in space relative to the SOBP in Figure 4a and listed in Table E5; corresponding results for carbon are shown in Figure 4b and Table E6. The mean thermal neutron fluence at the center of the SOBP is approximately 2.2×10^9 ($\pm 1.4 \times 10^8$) n/cm^2/Gy(RBE) for the carbon beam and 5.8×10^9 ($\pm 5.3 \times 10^7$) n/cm^2/Gy(RBE) for the helium beam.

In vitro evaluation of in-beam NCEPT

The fractions of T98G cells that remain viable after in-beam irradiation with helium and carbon ions are plotted as a function of increasing dose in Figure 5. Three treatment conditions were used for each ion: either no NCA, 500 μM [^{10}B]BPA, or 500 μM [^{157}Gd]DOTA-TPP.

The corresponding LD_{50} and LD90 doses estimated from the resazurin assay results and 10% and 1% survival fraction doses obtained from the clonogenic assay results are shown in Table 1.

In vitro evaluation of out-of-beam NCEPT

The fractions of T98G cells that remain viable after out-of-beam irradiation with helium and carbon ions are plotted as a function of increasing dose to the primary target in Figure 6. Cells were positioned within the phantom, immediately adjacent to the primary target volume and not in the path of the primary beam (at positions A and D shown in

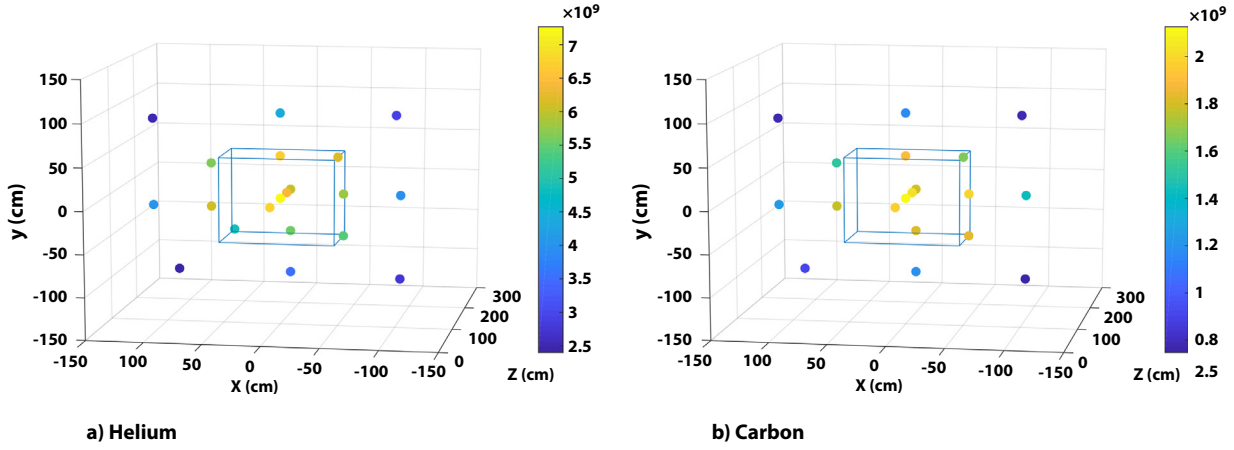

Fig. 4. Neutron fluence per unit dose (n/cm^2/Gy relative biological effectiveness) at the evaluated locations for helium (Fig. 4a) and carbon (Fig. 4b) ion beams. The wireframe rectangular prism represents the spread-out Bragg peak region.

Fig. 2). Again, 3 treatment conditions were used for each ion: either no NCA, 500 μM [^{10}B]BPA, or 500 μM [^{157}Gd] DOTA-TPP.

Effect of NCA concentration

The effect of NCA concentration on cell viability with a fixed in-beam helium and carbon ion dose is illustrated in Figure 7. half-maximal inhibitory concentration (IC50) values for [^{10}B]BPA with 3 Gy of carbon and helium ions were 9.33 and 30.04 μM, respectively. IC50 values for [^{157}Gd] DOTA-TPP with 3 Gy of carbon and helium ions were 21.72 and 8.89 μM, respectively.

In the absence of radiation, neither NCA is significantly cytotoxic in concentrations of up to 500 μM, although [^{nat}Gd]DOTA-TPP shows mild cytotoxicity at higher concentrations (>500 μM; Supplementary Materials Section 5).

Discussion

This paper presents the first experimental evidence quantifying the NCEPT effect in vitro.

Thermal neutron fluence was quantified at a range of positions inside and around the target volume via gold activation, demonstrating the presence of a clinically relevant thermal neutron field — the key enabling factor for NCEPT. The shape of the neutron fluence distribution is similar to that previously predicted via Monte Carlo simulations,[10] where the highest measured thermal neutron fluence is observed in the vicinity of the SOBP region before gradually falling off in all directions (Fig. 4). An estimation of the additional compound biological effectiveness (CBE)-weighted dose resulting from neutron capture can be derived from the estimated neutron fluence, using $D = \varphi \times \sigma_{NCA} \times N_{NCA} \times CBE$, where φ is the neutron fluence, σ_{NCA} denotes the fluence-to-kerma conversion factor, N_{NCA} represents the NCA concentration in ppm, and CBE signifies the compound biologic effectiveness, analogous to RBE for NCAs.[10] For [^{10}B]-BPA, with a CBE of 3.8, a σ_B of 8.86 $\times$ 10^{-14}, and a measured boron uptake of 202 ppm (refer to Table E10), alongside measured neutron fluences at the center of the SOBP of 5.8 $\times$ 10^9 n/cm^2/Gy (RBE) for helium ions and 2.2 $\times$ 10^9 n/cm^2/Gy(RBE) for carbon ions,[10] and assuming a clinical RBE of 2 for helium ions and 3 for carbon ions, the additional CBE-weighted dose because of neutron capture is 77% for helium ions and 44% for carbon ions, relative to the RBE-weighted dose from ion irradiation alone. In a similar calculation for [^{157}Gd]DOTA-TPP, assuming a CBE of 40,[40,41] σ_{Gd} = 9.27 $\times$ 10^{-15}, and a concentration of 419 ppm (see Table E10), the additional CBE-weighted dose is estimated at 180% for helium ions and 103% for carbon ions.

Human glioblastoma cells were placed both inside and immediately adjacent to a target volume inside a PMMA phantom, with and without the presence of 2 low-toxicity NCAs, [^{10}B]BPA and [^{157}Gd]DOTA-TPP[34,42] (Figs. 5-8). The target volume was irradiated with a 60- mm carbon or helium ion SOBP, both at a range of radiation doses with a fixed NCA dose, and second with a constant ion dose (corresponding to the ≅LD30 dose for cells not treated with NCAs) and a serial dilution of NCA. Cells placed inside the treatment volume reached 10% survival with the administration of 1.46 Gy of carbon ions or 1.67 Gy of helium ions with BPA and 1.37 Gy of carbon ions and 1.44 Gy of helium ions with [^{157}Gd]DOTA-TPP compared with 4.73 Gy of carbon ions and 6.53 Gy of helium ions with no NCA. This is a result of the combined effect of the dose delivered directly by the primary ion irradiation and the dose due to neutron capture by ^{10}B or ^{157}Gd. Therefore, dose enhancement to the treatment volume could be incorporated into treatment planning to either increase the effective dose to the tumor per ion delivered to the target or, where entrance dose is a concern, deliver an equivalent dose to the tumor with fewer ions. NCEPT will thus provide a wide range of potential options to the treating physician for either reducing off-target effects or increasing the dose that can be safely delivered to the target.

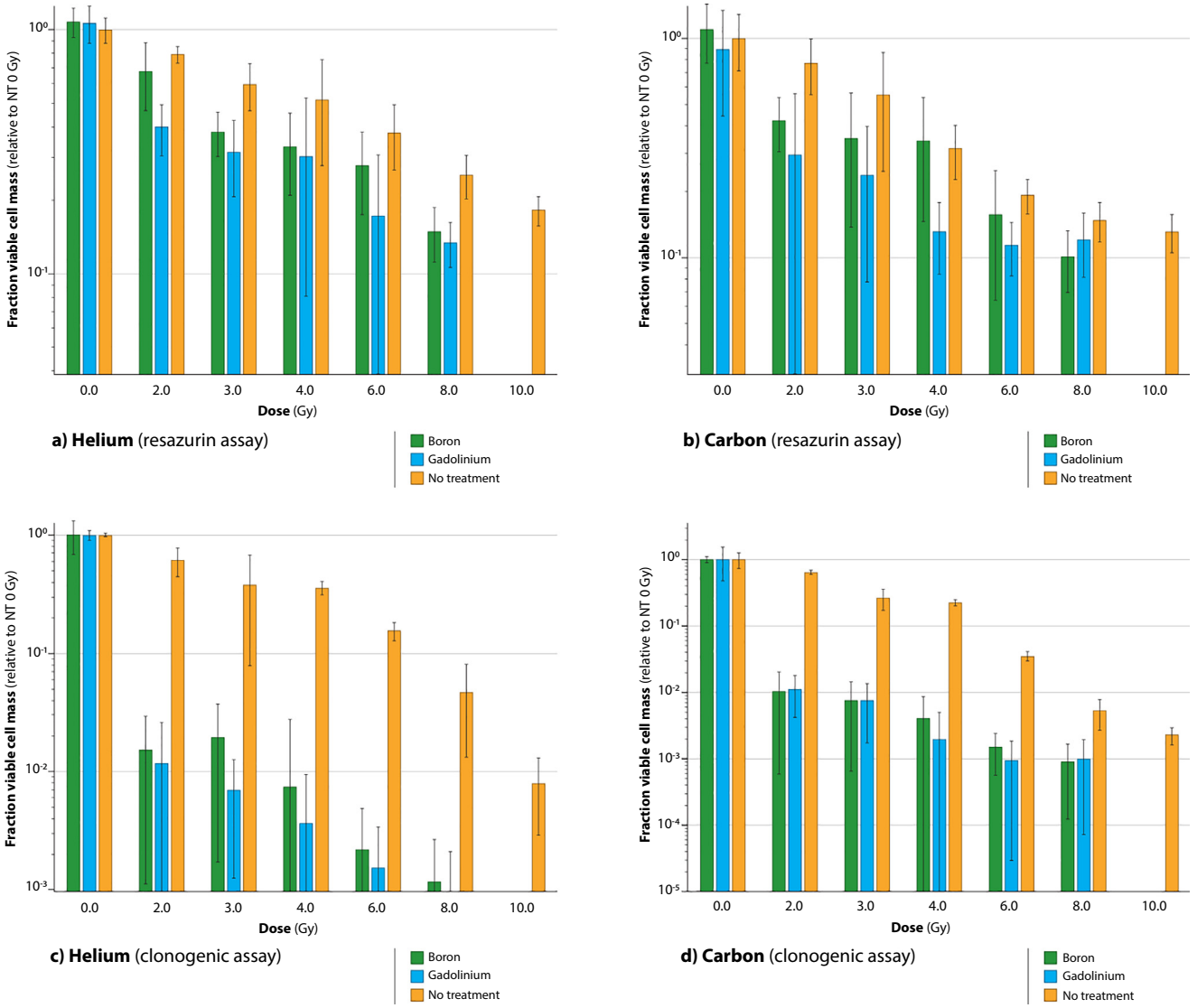

Fig. 5. Dose-dependent effect of neutron capture agents on cell survival. Cell survival fraction (normalized to no treatment, 0 Gy) for T98G cells positioned in the center of the spread out Bragg peak region and irradiated with helium ions (a, c) or carbon ions (b, d) across a range of physical radiation doses, after incubation with 500 μM of either neutron capture agent, in triplicate. Cell survival was evaluated using resazurin (a, b) and clonogenic (c, d) assays. Bars represent the mean fraction viable cell mass of 3 independent experiments for the clonogenic, and the resazurin assay shows representative data of 6 independent experiments. T-bars represent ±2 SDs.

Cells placed outside and adjacent to the treatment volume only exhibit a decrease in growth in response to escalating dose to the target when treated with either of the evaluated NCAs. The magnitude of the reduction in viability of NCA-treated cells outside the SOBP is similar to that observed after irradiation of NCA-treated cells within the SOBP for both helium and carbon ions (Fig. 5). Helium and carbon ions exhibit a lateral scattering of less than 2 mm at 11-cm depth in human tissue.[43] This superior dose conformity is demonstrated by the minimal response to escalating ion dose to target in cells that are not treated with an NCA, shown in Figure 6, while the neutron fluence at this location remains at 80% to 90% of the peak value (Fig. 4), suggesting that the dominant factor in the reduction in cell viability is the neutron capture process.

Comparing the in-beam dose response, it is evident that cells treated with 500-μM concentration of NCA show a much stronger dose response compared with the no-NCA control group. Obtaining a detailed cell survival response at very low ion dose values (ie, multiple steps in the 0-2 Gy dose range) presented experimental challenges. Modifying too many parameters at once, such as altering the attenuator to reduce dose rate, which also changes the beam quality, or extending the irradiation intervals for high-dose regimes at low-dose rates, would have compromised the experiment's integrity. Furthermore, varying the beam current wasn't a viable option because of limited beamtime at facilities like Heavy Ion Medical Accelerator in Chiba.

To navigate these constraints, we varied the neutron capture dose by titrating the NCA while keeping the ion dose

Table 1 Mean LD_{50} and LD90 of 6 independent experiments* and 10% and 1% survival fractions of 3 independent experiments†

Metric	Ion	No treatment	[^{10}B]BPA	[^{157}Gd]DOTA-TPP
LD_{50} dose	Helium	3.64 (0.41)	2.61 (0.07)	1.94 (0.13)
	Carbon	2.42 (0.11)	1.80 (0.11)	1.52 (0.49)
LD90 dose	Helium	13.09 (1.51)	8.92 (0.26)	5.22 (0.47)
	Carbon	13.58 (0.48)	7.79 (0.47)	3.91 (2.13)
10% survival fraction dose	Helium	6.53	1.67	1.44
	Carbon	4.73	1.46	1.37
1% survival fraction dose	Helium	9.88	3.36	2.89
	Carbon	7.99	2.91	2.75

T98G cells were placed at a depth of 110 mm in a 300 mm cubic polymethyl methacrylate phantom and irradiated in-beam, at the center of the SOBP60 (Fig. 3) with helium or carbon ions, either with neutron capture agents present (control), 500 μM [^{10}B]BPA or 500 μM [^{157}Gd]DOTA-TPP.

* Resazurin cell growth assay; see Figures 5a and 5b.

† Clonogenic assay, with survival thresholds estimated based on the fitted linear quadratic model curves in Figure 6.

constant (Fig. 7). Employing a dilution series of NCAs allowed us to elucidate the relative contribution of the neutron capture dose effectively, allowing us to evaluate cell viability in response to varying neutron doses at a finer resolution than would have been possible through coarse adjustments of the primary ion beam. For example, an NCA concentration of 10 μM used with a 3 Gy primary helium or carbon ion beam dose induces a 60% reduction of the viable cell mass, while a concentration of 100 μM with a 3-Gy primary beam dose results in a neutron capture effect equivalent to a 10-Gy dose of primary beam radiation (72% and 90% reduction in viable cell mass for helium and carbon ion beams, respectively).

Although the linear-quadratic model provides an excellent fit for the no-NCA clonogenic cell survival results, it is clearly unable to provide a satisfactory fit for the NCA-treated cells. Because the α and β parameters of the linear-quadratic model are constrained to be nonnegative, and the curve of best fit for the NCA-treated cells is concave up, the least-squares fit results in $\beta = 0$ in each case, such that the linear-quadratic model becomes a simple linear model. Because of the poor fit of this linear model across the full evaluated range of doses, to compute the 1% and 10% survival fraction doses we only consider the first 4 dose values, over which the logarithm of the survival fraction is approximately linear with respect to dose; while the fit remains

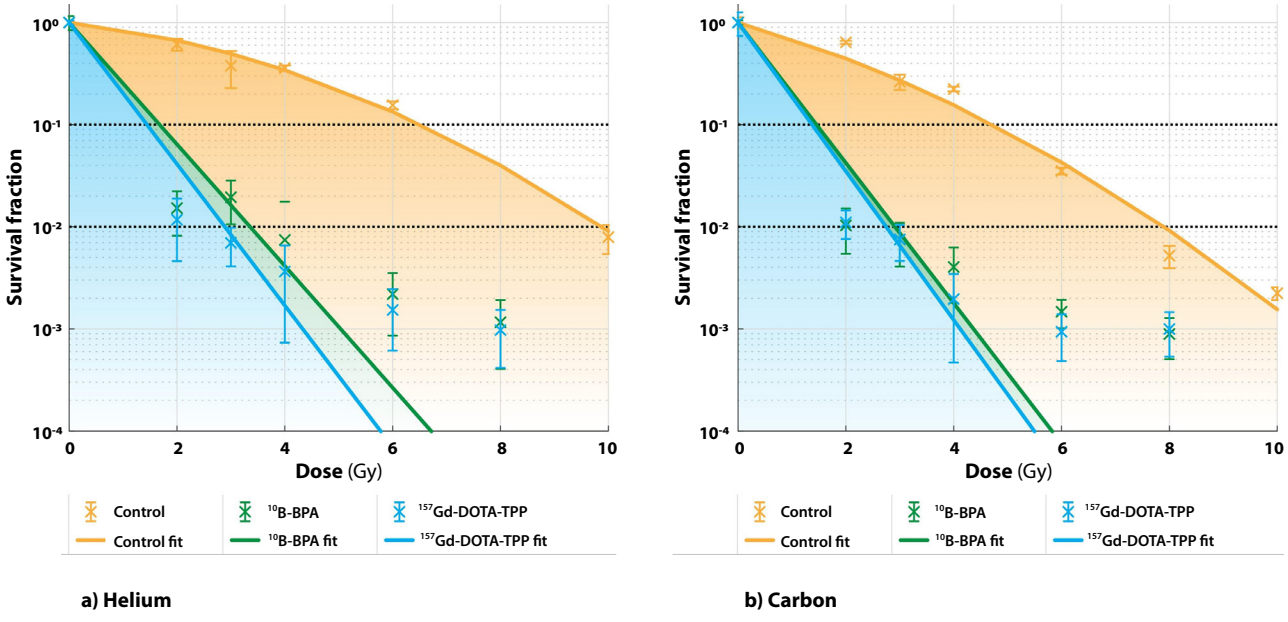

Fig. 6. Mean survival fractions as a function of dose (95% CIs) of 3 independent experiments for each population of cells treated with no neutron capture agent, [^{10}B]BPA or [^{157}Gd]DOTA-TPP, and irradiated with (a) helium and (b) carbon ion beams. The α and β parameters of the linear quadratic model were computed using a least-squares fitting process algorithm for each case (Table E8); 10% and 1% survival thresholds are shown as horizontal dashed lines.

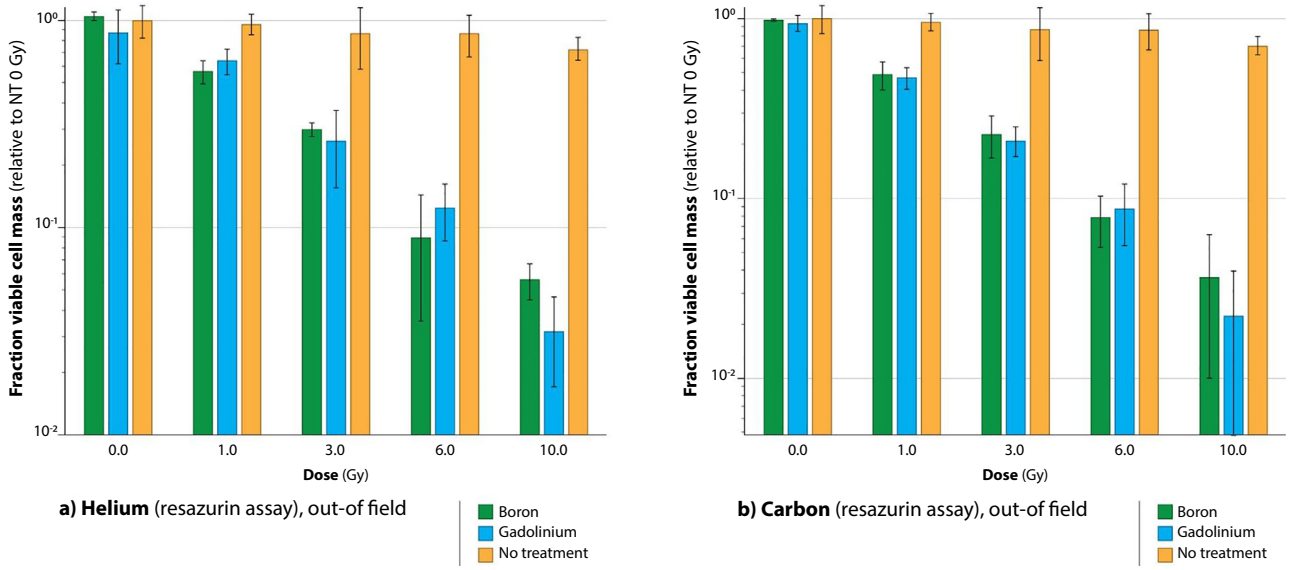

Fig. 7. Out-of-field effect of NCAs on cell survival. Fraction of viable cell mass (normalized to no treatment, 0 Gy) for T98G cells positioned outside of the target volume, to the left and right of the centroid of the spread out Bragg peak region, irradiated with (a) helium or (b) carbon across a range of physical radiation doses, after incubation with 500 μM of either NCA, in triplicate. Even at the highest in-beam dose of 10 Gy, the no-NCA controls only see a decrease in relative viable cell mass of about 15%. By contrast, cells incubated with either NCA experience a decline in viability as the target dose is escalated, decreasing by more than 95% for a primary dose of 10 Gy. Bars represent the mean fraction viable cell mass of 6 independent experiments for the resazurin assay, and the T-bars represent ±2 SDs.
Abbreviation: NCA = neutron capture agents.

poor, at least it allows an approximation of the 1% and 10% survival doses to be obtained. Relaxing the nonnegativity constraint results in a better fit but yields a nonsensical negative value for β.

Consider an absorbed helium ion dose of 3 Gy; the LQ model fit for the control group without NCA indicates a survival fraction of approximately 0.5 (50%). Based on the estimated dose enhancement factors obtained earlier, and assuming that the biologic effects of NCEPT are exclusively attributable to the additional neutron capture dose, the additional absolute doses due to neutron capture with [^{10}B]-BPA and [^{157}Gd]DOTA-TPP are estimated to be 2.31 and 5.41 Gy, respectively. These additional doses are expected to correspond to survival fractions of about 0.15 (15%) and 0.025 (2.5%). However, the experimental survival fractions obtained for the NCA-treated cells at 3 Gy are lower than these values — approximately 0.02 (2%) for [^{10}B]-BPA and 0.006 (0.6%) for [^{157}Gd]DOTA-TPP. In the case of 3 Gy of carbon ions, the extra doses are relatively lower: 1.32 Gy for [^{10}B]-BPA and 3.07 Gy for [^{157}Gd]DOTA-TPP, with survival fractions decreasing from approximately 0.2 (20%) (at 3 Gy, ions only) to 0.1 (10%) and 0.045 (4.5%) for [^{10}B]-BPA and [^{157}Gd]DOTA-TPP, respectively. Again, these figures are higher than the experimentally observed survival fractions at 3 Gy, which are around 0.008 (0.8%) for [^{10}B]-BPA and 0.007 (0.7%) for [^{157}Gd]DOTA-TPP. These findings suggest the presence of an additional, unaccounted for factor beyond the linear quadratic (LQ) model — potentially a nonlinear, combined effect involving multiple distinct biologic processes mediated by ions, neutrons, photons, and neutron-capture products. This complex interaction could lead to increased rates of cell death, surpassing what would be explained by a purely additive combination of the dose contributions from these 4 factors. Notably, similar results have been reported in the literature for certain cell lines treated with BPA-based boron neutron capture therapy (BNCT). For instance, Viegas et al[44] observed a dose response in UMR-106 osteosarcoma cells that is very similar to that seen in Figure 8 (in particular, the concave-up characteristic behavior that results in a straight-line fit because β is constrained to be nonnegative). The poor LQ model fitting for both BPA-BNCT and NCEPT experimental data suggests that both are incompletely described by the biophysical assumptions underlying the LQ model, a finding that supports previous criticism of the general validity of the model in the literature.[45,46]

Drawing on the principles of radionuclide therapy, we can envision a new class of radiopharmaceutical where the radiation emission within the biologic system is only triggered by an external radiation source, at a time and location determined by the treatment plan. NCEPT is fundamentally different from traditional radiosensitization techniques, as it introduces an entirely new radiation dose instead of merely amplifying a pre-existing one. Such an approach could deliver radiation more precisely to cellular targets while drastically reducing the dose to excretory pathways in comparison to current radionuclide therapeutics (which is a major limiting factor in such therapies). Future NCEPT

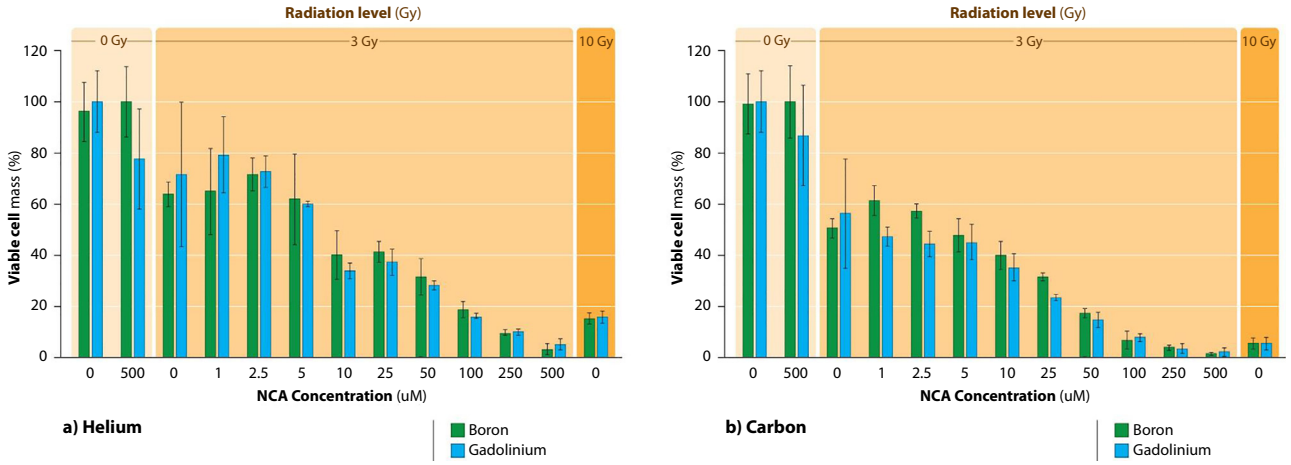

Fig. 8. Concentration-dependent effect of NCAs on cell viability. Viable cell mass (%) for T98G cells positioned in the center of the spread out Bragg peak region irradiated with (a) helium or (b) carbon, receiving a physical dose of 3 Gy and incubated with increasing concentrations of each NCA, in triplicate. Nonirradiated controls with 0 or 500 μM of each NCA were included along with a 10 Gy positive control. For comparison, a dose of 3 Gy delivered to cells incubated with a concentration of 100 to 250 μM of either NCA is roughly equivalent to a 10 Gy dose with no NCA present (right-most group). Bars represent the mean percentage viable cell mass of 2 independent experiments for the resazurin assay, and the T-bars represent $\pm$2 SDs.
Abbreviation: NCA = neutron capture agents.

agents should prioritize low inherent chemical toxicity and the targeted delivery of either ^{10}B to specific cellular or tissue sites or ^{157}Gd to specific organelle or cellular targets.

We note that the observed dose-enhancement effect shown in our experiments is clearly not related to proton fusion for several reasons. First, our radiation source is either ^{12}C or ^{4}He ions, and in both cases, no known projectile or target fragmentation reaction is able to generate protons in quantities sufficient to account for the observed results. Second, our target neutron capture isotopes, enriched ^{10}B or ^{157}Gd, are not conducive to beam-target fusion (and this would be the case even if a high-energy proton beam were used). Lastly, our findings, both in beam and out of beam, are entirely consistent with the measured neutron fluence surrounding the target, corroborating the work of Manandhar et al[16] and Hosobuchi et al,[17] who were unable to reproduce the purported proton-boron fusion dose-enhancement results, and the corresponding Monte Carlo simulation results of Jacobsen et al[13] and Khaledi et al,[14] which predict negligible dose enhancement during proton irradiation of a ^{11}B-loaded target. We note that our observed results further support the hypothesis that the previously observed proton-(natural)-boron dose enhancement effect is likely due to neutron capture by ^{10}B, which constitutes approximately 19.8% of natural boron, because it is expected that similar (or even greater) thermal neutron fluences to those observed in these experiments would exist around the target when irradiated at depth.

The results obtained to date provide strong justification for proceeding to in vivo experimental exploration of NCEPT. The data suggest the potential for ion doses administered during particle therapies should be reduced, which will result in a corresponding reduction in normal tissue complications and unwanted side effects of radiation on sensitive organs. Because the dose to target can be achieved with a lower ion dose, NCEPT will enable treatment to be completed with fewer fractions (analogous to hypofractionation). Because of the short treatment time of particle therapy relative to NCT (a few minutes as opposed to >1 hour), NCEPT treatment can be performed without needing to maintain the NCA concentration in the patient for an extended period. However, it would be necessary to study the possibility of administering high doses of BPA in successive fractions, as BNCT is usually carried out in 1 session only, requiring at least 350 mg/kg of BPA with a 2-hour infusion before (and sometimes during) neutron irradiation.[47] Additionally, this work provides further impetus to investigate the potential of NCEPT in proton therapy. Previous simulation studies indicated that neutron fluence during proton therapy should be even higher than for carbon ion therapy, which would imply that the effect of NCEPT may be even more significant there.[10] The experimental results presented in this work strongly support that hypothesis; we have shown that helium ion beams generate a substantially larger thermal neutron fluence for a given biologic dose compared with carbon ions. Given the wider availability of proton therapy compared with heavy ion therapy, this would also expand the availability of NCEPT to a much wider range of potential patients and diseases.

Conclusion

NCEPT represents a new paradigm in charged particle therapy. The combination of biochemically targeted neutron-capturing pharmaceuticals with conformally targeted charged particle therapy — in particular, through

exploitation of an internally generated secondary/tertiary radiation field — gives the possibility of attaining a remarkably high specificity of energy deposition within cells and tissues. The utility of neutron capture has been shown to extend beyond the margins of the conventional image-targeted treatment volume and provides an opportunity to target undiagnosed cancer microinfiltrates that are otherwise left untreated. NCEPT highlights the potential of low molecular weight, high specificity small molecules, labeled with ^{10}B, for a much broader range of radiotherapeutic and radiosensitization applications — an area previously underexplored in comparison with heavier elements and large molecules or nanoparticles. We have demonstrated the potential to repurpose existing pharmaceuticals ([^{10}B]BPA), as well as the potential for novel compounds ([^{157}Gd]DOTA-TPP), to increase the efficacy of existing charged particle beams. The therapeutic exploitation of internally generated neutrons by neutron capture agents is a process hitherto entirely unexplored by medicinal chemists, biologists, and pharmacologists. We strongly feel that its potential for affecting clinical outcomes and improving quality of life after treatment warrants further investigation.

References

1. Loeffler JS, Durante M. Charged particle therapy—optimization, challenges and future directions. *Nat Rev Clin Oncol* 2013;10:411-424.
2. Durante M, Paganetti H. Nuclear physics in particle therapy: A review. *Rep Prog Phys* 2016;79 096702.
3. PTCOG. Facilities in operation. Available at: https://www.ptcog.ch/index.php/facilities-in-operation. Accessed December 15, 2023.
4. Battistoni G, Mattei I, Muraro S. Nuclear physics and particle therapy. *Adv Phys* 2016;1:661-686.
5. Zeitlin C, Tessa CL. The role of nuclear fragmentation in particle therapy and space radiation protection. *Front Oncol* 2016;6:65.
6. Hu K, Yang Z, Zhang L, et al. Boron agents for neutron capture therapy. *Coord Chem Rev* 2020;405 213139.
7. Sauerwein WAG. Principles and roots of neutron capture therapy. In: Sauerwein W, Wittig A, Moss R, Nakagawa Y, eds. *Neutron Capture Therapy: Principles and Applications*. Springer; 2012:1-16.
8. Yamamoto T, Nakai K, Matsumura A. Boron neutron capture therapy for glioblastoma. *Cancer Lett* 2008;262:143-152.
9. Issa F, Ioppolo JA, Rendina LM. 3.30 - Boron and gadolinium neutron capture therapy. In: Reedijk J, Poeppelmeier K, eds. *Comprehensive Inorganic Chemistry II*. 2nd ed.Elsevier; 2013:877-900.
10. Safavi-Naeini M, Chacon A, Guatelli S, et al. Opportunistic dose amplification for proton and carbon ion therapy via capture of internally generated thermal neutrons. *Sci Rep* 2018;8:16257.
11. Cirrone GAP, Manti L, Margarone D, et al. First experimental proof of Proton Boron Capture Therapy (PBCT) to enhance protontherapy effectiveness. *Sci Rep* 2018;8:1141.
12. Bláha P, Feoli C, Agosteo S, et al. The proton-boron reaction increases the radiobiological effectiveness of clinical low- and high-energy proton beams: Novel experimental evidence and perspectives. *Front Oncol* 2021;11 682647.
13. Jacobsen VL, Johansen JG, Fynbo HOU, Bassler N. A Monte Carlo study of high-LET particle production in proton boron therapy. *Eur Phys J Plus* 2023;138:625.
14. Khaledi N, Wang X, Hosseinabadi RB, Samiei F. Is the proton−boron fusion therapy effective? *J Radiother Pract* 2021;20:153-157.
15. Meija J, Coplen TB, Berglund M, et al. Isotopic compositions of the elements 2013 (IUPAC Technical Report). *Pure Appl Chem* 2016;88:293-306.
16. Manandhar M, Bright SJ, Flint DB, et al. Effect of boron compounds on the biological effectiveness of proton therapy. *Med Phys* 2022;49:6098-6109.
17. Hosobuchi M, Kataoka J, Yokokawa H, et al. Experimental verification of efficacy of pBCT in terms of physical and biological aspects. *Nucl Instrum Methods Phys Res* 2023;1045 167537.
18. Dymova MA, Taskaev SY, Richter VA, Kuligina EV. Boron neutron capture therapy: Current status and future perspectives. *Cancer Commun* 2020;40:406-421.
19. Wongthai P, Hagiwara K, Miyoshi Y, et al. Boronophenylalanine, a boron delivery agent for boron neutron capture therapy, is transported by ATB0,+, LAT1 and LAT2. *Cancer Sci* 2015;106:279-286.
20. Kanai Y. Amino acid transporter LAT1 (SLC7A5) as a molecular target for cancer diagnosis and therapeutics. *Pharmacol Ther* 2022;230 107964.
21. Soloway AH, Barth RF, Gahbauer RA, Blue TE, Goodman JH. The rationale and requirements for the development of boron neutron capture therapy of brain tumors. *J Neurooncol* 1997;33:9-18.
22. Murphy MP. Selective targeting of bioactive compounds to mitochondria. *Trends Biotechnol* 1997;15:326-330.
23. Fulda S, Galluzzi L, Kroemer G. Targeting mitochondria for cancer therapy. *Nat Rev Drug Discov* 2010;9:447-464.
24. Battogtokh G, Choi YS, Kang DS, et al. Mitochondria-targeting drug conjugates for cytotoxic, anti-oxidizing and sensing purposes: Current strategies and future perspectives. *Acta Pharm Sin B* 2018;8:862-880.
25. Dairkee SH, Hackett AJ. Differential retention of rhodamine 123 by breast carcinoma and normal human mammary tissue. *Breast Cancer Res Treat* 1991;18:57-61.
26. Goorley T, Nikjoo H. Electron and photon spectra for three gadolinium-based cancer therapy approaches. *Radiat Res* 2000;154:556-563.
27. Golshani M, Mowlavi AA, Azadegan B. Gadolinium neutron capture therapy: Calculation of 157Gd kerma factor and a dosimetry study using MCNP Monte Carlo code. *Radiat Phys Chem* 2022;197 110155.
28. Cerullo N, Bufalino D, Daquino G. Progress in the use of gadolinium for NCT. *Appl Radiat Isot* 2009;67:S157-S160.
29. Enger SA, Giusti V, Fortin M-A, Lundqvist H, af Rosenschöld PM. Dosimetry for gadolinium neutron capture therapy (GdNCT). *Radiat Meas* 2013;59:233-240.
30. Ghosh N, Sil PC. Mitochondria and apoptosis. In: de Oliveira MR, ed. *Mitochondrial Physiology and Vegetal Molecules*. Academic Press; 2021:127-149.
31. Weinberg AM, Wigner EP. *The Physical Theory of Neutron Chain Reactors*. University of Chicago Press; 1958.
32. Duderstadt JJ, Hamilton LJ. *Nuclear Reactor Analysis*. John Wiley & Sons; 1976.
33. Kobayashi K, Yamamoto S, Kimura I, Miki R, Itoh T. Measurement of neutron flux spectrum by multi-foil activation method at the central graphite cavity of UTR-KINKI. *Kinki Daigaku Genshiryoku Kenkyusho Nenpo Jpn* 1988;25.
34. Morrison DE, Aitken JB, de Jonge MD, Issa F, Harris HH, Rendina LM. Synthesis and biological evaluation of a class of mitochondrially-targeted gadolinium(III) agents. *Chemistry* 2014;20:16602-16612.
35. Anoopkumar-Dukie S, Carey JB, Conere T, O'sullivan E, van Pelt FN, Allshire A. Resazurin assay of radiation response in cultured cells. *Br J Radiol* 2005;78:945-947.
36. Czekanska EM. Assessment of cell proliferation with resazurin-based fluorescent dye. In: Stoddart MJ, ed. *Mammalian Cell Viability: Methods and Protocols*. Humana Press; 2011:27-32.
37. Rosenblum ML, Knebel KD, Wheeler KT, Barker M, Wilson CB. Development of an in vitro colony formation assay for the evaluation of in vivo chemotherapy of a rat brain tumor. *In Vitro* 1975;11:264-273.

38. GE Healthcare. ImageQuant LAS 4000 series. Available at: https://www.gelifesciences.com/ko/kr/shop/molecular-biology/nucleic-acid-electrophoresis−blotting−and-detection/molecular-imaging-for-nucleic-acids/imagequant-las-4000-series-p-00039. Accessed December 15, 2023.
39. Geissmann Q. OpenCFU, a new free and open-source software to count cell colonies and other circular objects. *PLoS One* 2013;8:e54072.
40. Zamenhof R, Brenner J, Yanch J, et al. Treatment planning for neutron capture therapy of glioblastoma multiforme using an epithermal neutron beam from the Mitr-II research reactor and Monte Carlo simulation. In: Allen BJ, Moore DE, Harrington BV, eds. *Progress in Neutron Capture Therapy for Cancer*. Springer; 1992:173-177.
41. Kanai T, Matsufuji N, Miyamoto T, et al. Examination of GyE system for HIMAC carbon therapy. *Int J Radiat Oncol* 2006;64:650-656.
42. Morrison DE, Aitken JB, de Jonge MD, Ioppolo JA, Harris HH, Rendina LM. High mitochondrial accumulation of new gadolinium(III) agents within tumour cells. *Chem Commun* 2014;50:2252-2254.
43. Kraft G. Tumortherapy with ion beams. *Nucl Instrum Methods Phys Res* 2000;454:1-10.
44. Viegas AMD, Postuma I, Bortolussi S, et al. Detailed dosimetry calculation for in-vitro experiments and its impact on clinical BNCT. *Phys Med* 2021;89:282-292.
45. McMahon SJ. The linear quadratic model: Usage, interpretation and challenges. *Phys Med Biol* 2018;64:01TR01.
46. Kirkpatrick JP, Brenner DJ, Orton CG. The linear-quadratic model is inappropriate to model high dose per fraction effects in radiosurgery. *Med Phys* 2009;36:3381-3384.
47. IAEA. *Advances in Boron Neutron Capture Therapy*. IAEA; 2023.